第 17 卷第 3 期 2019 年 6 月
1672-6553/2019/17(3)/270-11

动力学与控制学报
JOURNAL OF DYNAMICS AND CONTROL

Vol.17 No.3
Jun. 2019

石墨烯三相复合材料板的非线性动力学研究*

姜盼　郭翔鹰†　张伟

(北京工业大学 机电学院,北京　100124)

摘要　研究带有石墨烯涂层的 1-3 型压电纤维复合材料(MFC-GP)简支板结构的非线性动力学特性. 首先,基于 Reddy 一阶剪切变形理论、Von Kármán 位移应变关系以及 Hamilton 原理,推导了 MFC-GP 复合材料板的非线性偏微分方程. 根据边界条件选择适当的模态函数,利用 Galerkin 法将偏微分方程离散成两自由度的常微分方程. 采用多尺度方法进行摄动分析,得到结构在 1:1内共振下的频响方程,分析了石墨烯体积分数、电压、温度等对结构非线性频响曲线的影响. 通过数值模拟,运用分叉图、相图、波形图研究了外激励对 MFC-GP 板非线性振动响应的影响. 结果表明:不同参数及外激励下,结构出现了复杂的非线性动力学行为,对今后的工程实际应用具有一定的指导意义.

关键词　MFC-GP 板,　内共振,　频响曲线,　非线性振动

DOI:　10.6052/1672-6553-2019-021

引言

石墨烯是由 Geim 课题组用撕胶带法将高定向石墨进行剥离而发现的,它是以 sp^2 碳原子以蜂巢晶格构成的二维单原子层结构,如图 1 所示.独特的结构使其具有优异的力学、电学、热学性能,尤其在航空航天领域中有巨大的发展前景[1,2].

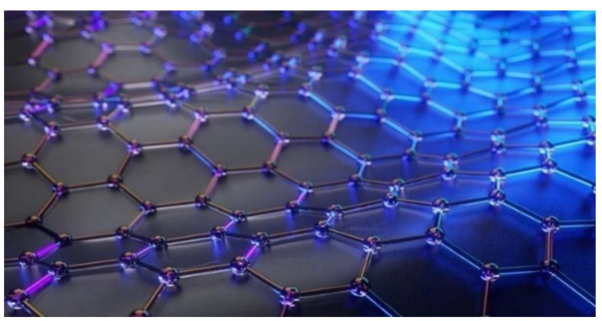

图 1　石墨烯结构示意图

Fig.1　Schematic diagram of thegraphene structure

目前,关于石墨烯复合材料的非线性动力学特性的研究引起了国内外学者的广泛关注.Adak 等人[3]研究了石墨烯和环氧树脂复合材料的静态和动态力学性质.Shen 等人[4]研究了石墨烯增强复合材料梯度梁在热环境下的非线性振动.结果表明,石墨烯增强剂的梯度分布可改变梁的刚度和振动响应,同时随着温度增加结构的非线性频率增加. Shahrjerdi 等人[5]研究了石墨烯纳米复合材料梯度梁的自由振动,考虑了纳米板的分布函数、质量分数、尺度效应、温度对固有频率的影响.Li 等人[6]研究了石墨烯-弹-压电层合薄膜作为纳米质量探测器的非线性频移行为,结果表明,非线性和非局部参数对 GEP 层合纳米质量探测器的频移均有影响,当不同质量粒子附着在探测器表面时,可以通过调节作用于压电层的外部电压来控制频移.Xu 等人[7]发现了石墨烯具有压电特性.Phiri 等人[8]研究了石墨烯、氧化石墨烯、氧化还原石墨烯的力学、热学、电学性能,结果表明,氧化石墨烯不具有压电特性.Guo 等人[9]研究了石墨烯压电纤维复合材料悬臂板的非线性动力学特性.

压电纤维复合材料在振动控制、变形控制和颤振抑制等方面都有广泛的作用[10]. 目前,国内外对压电纤维复合材料的非线性振动特性做了大量的研究. 郭翔鹰等人[11]建立了 MFC 层合壳的非线性动力学模型,研究了横向激励和压电性能对结构稳定性的影响. 杨佳慧等人[12]分析了压电复合材料悬臂板在 1:3内共振下非线性动力学行为. Ray 等

2018-11-04 收到第 1 稿,2018-12-21 收到修改稿.
* 国家自然科学基金资助项目(11772010,11572006,11602234)
† 通讯作者 E-mail:eagle2008guo@yeah.net

人[13]采用了压电纤维增强复合材料的阻尼层,研究了约束层和压电纤维取向对复合材料层合薄壳振动的影响. Rafiee 等人[14]研究了表面粘合压电驱动器的碳纳米管复合材料板的非线性自由振动响应.

综上所述,对于石墨烯复合材料和压电纤维复合材料的研究较多,但研究石墨烯和压电纤维复合材料形成三相复合材料的文献较少. 本文考虑在 1-3 型压电纤维复合材料板的上、下表面添加多层片状的石墨烯,形成多组分复合材料(MFC-GP),分析了石墨烯体积分数、电压、温度、初相位对结构非线性振动响应的影响. 最后通过数值模拟,研究了外激励对结构的非线性动力学行为的影响.

1　MFC-GP 复合材料板的动力学方程

考虑在 1-3 型压电纤维复合材料板的上、下表面添加多层片状石墨烯,如图 2 所示.

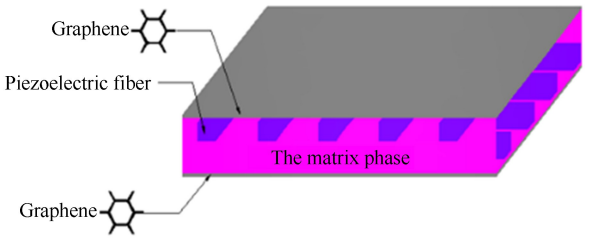

图 2　结构示意图

Fig.2　Schematic diagram of the structure

根据文献[4,9,15],MFC-GP 复合材料板的杨氏模量、泊松比、热膨胀系数分别可通过不同组分材料的混合率公式表示为

$$E_c=E_g a_g+(1-a_g)(E_p a_p+(1-a_p)E_m) \tag{1}$$

其中,E_g、E_p 和 E_m 分别是石墨烯、压电纤维、环氧树脂的杨氏模量; a_g 和 a_p 分别是石墨烯、压电纤维的体积分数.

$$\upsilon=\upsilon_g a_g+(1-a_g)(\upsilon_p a_p+(1-a_p)\upsilon_m) \tag{2}$$

这里,υ_g、υ_p 和 υ_m 分别是石墨烯、压电纤维、环氧树脂的泊松比.

$$\alpha=\alpha_g a_g+(1-a_g)(\alpha_p a_p+(1-a_p)\alpha_m) \tag{3}$$

其中,α_g、α_p 和 α_m 分别是石墨烯、压电纤维、环氧树脂的热膨胀系数.

$$E_3=\frac{U}{t_g}a_g+(1-a_g)\frac{U}{t_p}a_p \tag{4}$$

这里,U 是外接电压,t_g 和 t_p 分别是石墨烯和压电纤维的厚度.

整体材料的压电应变系数通过如下方式得到

$$d_{3i}=\frac{M_i}{N_i}\quad (i=1,2) \tag{5}$$

M_i 和 N_i 是关于压电常数(g_i),体积分数(a_g,a_p),柔性系数(s_i),介电隔离率矩阵(β_i^T)的表达式,具体表达式见附录 A.

根据以上得到的参数,可将 MFC-GP 板的应力-应变关系表示为

$$\begin{Bmatrix}\sigma_1\\ \sigma_2\\ \sigma_4\\ \sigma_5\\ \sigma_6\end{Bmatrix}=\begin{bmatrix}Q_{11}&Q_{12}&0&0&0\\ Q_{21}&Q_{22}&0&0&0\\ 0&0&Q_{44}&0&0\\ 0&0&0&Q_{55}&0\\ 0&0&0&0&Q_{66}\end{bmatrix}\cdot \left\{\begin{bmatrix}\varepsilon_{xx}\\ \varepsilon_{yy}\\ 0\\ 0\\ \gamma_{xy}\end{bmatrix}-\begin{bmatrix}\alpha\\ \alpha\\ 0\\ 0\\ 0\end{bmatrix}\Delta T-\begin{bmatrix}d_{31}\\ d_{32}\\ 0\\ 0\\ 0\end{bmatrix}E_3\right\} \tag{6}$$

其中,$Q_{11}=\dfrac{E_c}{1-\upsilon^2}=Q_{22}$, $Q_{12}=\dfrac{\upsilon E_c}{1-\upsilon^2}=Q_{21}$,

$$Q_{44}=Q_{55}=Q_{66}=\frac{E_c}{2(1-\upsilon)}$$

考虑长为 a,宽为 b,厚度为 h 的复合材料板,受横向载荷 $F\cos(\Omega t)$ 作用. 同时考虑电压和热载荷作用,如图 3 所示. 直角坐标系在 MFC-GP 板的中面,(u,v,w) 和 (u_0,v_0,w_0) 分别表示 MFC-GP 板上的任意一点位移和板中面任意一点位移.

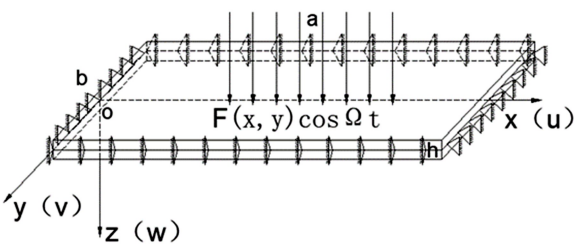

图 3　MFC-GP 板的力学模型

Fig.3　Mechanical model of MFC-GP plate

根据 Reddy 一阶剪切变形理论,MFC-GP 的位移场可表示为

$$u(x,y,z,t)=u_0(x,y,t)-z\varphi_x(x,y,t) \tag{7}$$

$$v(x,y,z,t)=v_0(x,y,t)-z\varphi_y(x,y,t) \tag{8}$$

$$w(x,y,z,t)=w_0(x,y,t) \tag{9}$$

根据 Von Kármán 位移应变关系,可得到

$$\varepsilon_{xx}=\frac{\partial u_0}{\partial x}+\frac{1}{2}\left(\frac{\partial w_0}{\partial x}\right)^2-z\frac{\partial^2 w_0}{\partial x^2} \tag{10}$$

$$\varepsilon_{yy}=\frac{\partial v_0}{\partial y}+\frac{1}{2}\left(\frac{\partial w_0}{\partial y}\right)^2-z\frac{\partial^2 w_0}{\partial y^2} \tag{11}$$

$$\gamma_{xy}=\frac{\partial u_0}{\partial y}+\frac{\partial v_0}{\partial x}+\frac{\partial w_0}{\partial x}\frac{\partial w_0}{\partial y}-2z\frac{\partial^2 w_0}{\partial x\partial y} \tag{12}$$

将(7)~(12)带入 Hamilton 原理,其表达式如下:

$$\delta\int_{t_0}^{t_1}(T-U+W)dt=0 \tag{13}$$

得到广义位移形式表示的非线性动力学方程:

$$a_{11}\frac{\partial^2 u_0}{\partial x^2}+a_{12}\frac{\partial w_0}{\partial x}\frac{\partial^2 w_0}{\partial x^2}+a_{13}\frac{\partial^2 v_0}{\partial x\partial y}+a_{14}\frac{\partial w_0}{\partial y}\frac{\partial^2 w_0}{\partial x\partial y}+a_{15}\frac{\partial^2 u_0}{\partial y^2}+a_{16}\frac{\partial w_0}{\partial x}\frac{\partial^2 w_0}{\partial y^2}=a_{17}\frac{\partial^2 u_0}{\partial t^2}+a_{18}\frac{\partial^3 w_0}{\partial t^2\partial x} \tag{14}$$

$$b_{11}\frac{\partial^2 v_0}{\partial y^2}+b_{12}\frac{\partial w_0}{\partial y}\frac{\partial^2 w_0}{\partial y^2}+b_{13}\frac{\partial^2 u_0}{\partial x\partial y}+b_{14}\frac{\partial w_0}{\partial x}\frac{\partial^2 w_0}{\partial x\partial y}+b_{15}\frac{\partial^2 v_0}{\partial x^2}+b_{16}\frac{\partial w_0}{\partial y}\frac{\partial^2 w_0}{\partial x^2}=b_{17}\frac{\partial^2 v_0}{\partial t^2}+b_{18}\frac{\partial^3 w_0}{\partial t^2\partial y} \tag{15}$$

$$c_{11}\frac{\partial w_0}{\partial x}\frac{\partial w_0}{\partial y}\frac{\partial^2 w_0}{\partial x\partial y}+c_{12}\frac{\partial w_0}{\partial x}\frac{\partial^2 u_0}{\partial y^2}+c_{13}\frac{\partial u_0}{\partial x}\frac{\partial^2 w_0}{\partial^2 y}+c_{14}\frac{\partial w_0}{\partial x}\frac{\partial^2 u_0}{\partial^2 x}+c_{15}\left(\frac{\partial w_0}{\partial x}\right)^2\frac{\partial^2 w_0}{\partial y^2}+c_{16}\frac{\partial u_0}{\partial x}\frac{\partial^2 w_0}{\partial x^2}+c_{17}\frac{\partial u_0}{\partial y}\frac{\partial^2 w_0}{\partial x\partial y}+c_{18}\left(\frac{\partial w_0}{\partial y}\right)^2\frac{\partial^2 w_0}{\partial^2 x}+c_{19}\left(\frac{\partial w_0}{\partial x}\right)^2\frac{\partial^2 w_0}{\partial^2 x}+c_{20}\frac{\partial v_0}{\partial y}\frac{\partial^2 w_0}{\partial y^2}+c_{21}\frac{\partial w_0}{\partial y}\frac{\partial^2 u_0}{\partial x\partial y}+c_{22}\frac{\partial w_0}{\partial x}\frac{\partial^2 v_0}{\partial x\partial y}+c_{23}\left(\frac{\partial w_0}{\partial y}\right)^2\frac{\partial^2 w_0}{\partial^2 y}+c_{24}\frac{\partial w_0}{\partial y}\frac{\partial^2 v_0}{\partial^2 y}+c_{25}\frac{\partial v_0}{\partial y}\frac{\partial^2 w_0}{\partial x^2}+c_{26}\frac{\partial w_0}{\partial y}\frac{\partial^2 v_0}{\partial x^2}+c_{27}\frac{\partial v_0}{\partial x}\frac{\partial^2 w_0}{\partial x\partial y}+c_{28}\frac{\partial^2 w_0}{\partial^2 x}+c_{29}\frac{\partial^2 w_0}{\partial^2 y}+c_{30}\frac{\partial^4 w_0}{\partial^4 x}+c_{31}\frac{\partial^4 w_0}{\partial x^2\partial y^2}+c_{32}\frac{\partial^4 w_0}{\partial y^4}+F\cos(\Omega t)+c_{33}\ddot{w}_0=c_{34}\ddot{w}_0+c_{35}\frac{\partial\ddot{u}_0}{\partial x}+c_{36}\frac{\partial\ddot{v}_0}{\partial y}+c_{37}\frac{\partial^2\ddot{w}_0}{\partial x^2}+c_{38}\frac{\partial^2\ddot{w}_0}{\partial y^2} \tag{16}$$

其中,$F\cos(\Omega t)$ 为外激励,a_{ij},b_{ij},c_{ij} 表达式见附录 B.

2 Galerkin 离散

四边简支情况下的 MFC-GP 板,边界条件为:

$$x=0,a:w=0,\frac{\partial^2 w}{\partial x^2}=0 \tag{17}$$

$$y=0,b:w=0,\frac{\partial^2 w}{\partial y^2}=0 \tag{18}$$

根据文献[16],引入无量纲参数,对方程(14)~(16)进行无量纲化

$$\bar{w}=\frac{w_0}{h},\bar{u}=\frac{u_0}{a},\bar{v}=\frac{v_0}{b},\bar{F}=\frac{(ab)^{\frac{7}{2}}}{Eh^7}F,$$

$$\bar{x}=\frac{x}{a},\bar{y}=\frac{y}{b},\bar{A}_{ij}=\frac{(ab)^{\frac{1}{2}}}{Eh^2}A_{ij},\bar{D}_{ij}=\frac{(ab)^{\frac{1}{2}}}{Eh^4}D_{ij},$$

$$\bar{I}_{ij}=\frac{1}{(ab)^{\frac{i+1}{2}}\rho}I_{ij},\bar{t}=\pi^2\left(\frac{E}{ab\rho}\right)^{\frac{1}{2}}t \tag{19}$$

根据边界条件,MFC-GP 板的横向位移的解可表示为

$$w(x,y,t)=\sum_{m=1}^{\infty}\sum_{n=1}^{\infty}w_{mn}(t)\sin\frac{m\pi x}{a}\sin\frac{n\pi y}{b} \tag{20}$$

利用 Galerkin 将横向位移进行一阶离散,得到无量纲后的常微分方程:

$$\ddot{w}+\lambda\dot{w}+\zeta_1 w^3+\omega^2 w+(t\cos(\Omega_2 t)+p\cos(\Omega_3 t))w=\zeta_2 F\cos(\Omega_1 t) \tag{21}$$

其中,λ 为阻尼系数,ζ_1 为非线性项系数,t、p 分别为温度系数,压电系数.

将方程(21)改写成如下形式:

$$\Lambda_1=w \tag{22}$$

$$\Lambda_2=\dot{w} \tag{23}$$

$$\frac{\partial\Lambda_1}{\partial t}=\Lambda_2 \tag{24}$$

$$\frac{\partial\Lambda_2}{\partial t}=-\omega^2\Lambda_1-(t\cos(\Omega_2 t)+p\cos(\Omega_3 t))\Lambda_1+\xi_2 F\cos(\Omega_1 t) \tag{25}$$

将上式(22)~(25)写成矩阵形式:

$$\dot{\boldsymbol{\Lambda}}_i=\begin{bmatrix}0&1\\ \Pi&0\end{bmatrix}\boldsymbol{L}_j+\begin{bmatrix}0\\ Y\end{bmatrix}\quad(i,j=1,2) \tag{26}$$

令

$$\boldsymbol{J}=\begin{bmatrix}0&1\\ \Pi&0\end{bmatrix} \tag{27}$$

其中,$\Pi=-\omega^2-t\cos(\Omega_2 t)-p\cos(\Omega_3 t)$

$\gamma=\xi_2 F\cos(\Omega_1 t)$

当矩阵 $\boldsymbol{J}$ 的所有特征值实部小于零,系统稳定,此时虚部为系统的固有圆频率.选取表 1 参数,得到不同 m、n 下的固有频率,如表 2 所示.

表 1　MFC-GP 板的物理参数

Table 1　The Physical parameters of MFC-GP plates

Material properties	Epoxy	GPL	MFC
Young's modulus (GPa)	3.0	1010	210
Density (kg m^{-3})	1200	1062.5	7450
Poisson's ratio	0.34	0.186	0.3
Dielectric constant (C/m^2)	$\varepsilon_{11}=10$	$\varepsilon_{33}=726$	$\varepsilon_{33}=350$
Piezo-electrical-strain coefficient (pC/N)	0	$d_{31}=-250$ $d_{32}=200$ $d_{33}=600$	$d_{31}=-250$ $d_{32}=300$ $d_{33}=1400$
Flexibility coefficient (10^{-12} m^2/N)	$s_{11}=185.6$ $s_{12}=-360.3$	$s_{11}=0.8$ $s_{12}=-3.6$	$s_{11}=3.5$ $s_{12}=-8.3$

表 2　不同 m、n 情况下 MFC-GP 板固有频率

Table 2　Natural frequencies of MFC-GP plates under the case of different m and n

Modes	a_g		
	0	0.005	0.05
$m=1,n=1$	1.96	1.97	2.03
$m=1,n=2$	3.36	3.46	4.25
$m=2,n=1$	2.84	3.02	4.18
$m=2,n=2$	3.97	4.20	5.72
$m=1,n=3$	4.85	4.95	5.78
$m=3,n=1$	3.79	3.84	4.15

从表 2 中可以得到,当 $m=1,n=2$、$m=2,n=1$ 时,结构存在 1:1内共振.

将横向位移进行二阶离散,形式如下:

$$w(x,y,t)=w_1(t)\sin\left(\frac{\pi x}{a}\right)\sin\left(\frac{2\pi y}{b}\right)+w_2(t)\sin\left(\frac{2\pi x}{a}\right)\sin\left(\frac{\pi y}{b}\right) \tag{28}$$

同时,将外激励,压电力,温度力进行二阶离散,形式如下:

$$F(x,y,t)=F_1(t)\cos(\Omega_1 t)\sin\left(\frac{\pi x}{a}\right)\sin\left(\frac{2\pi y}{b}\right)+F_2(t)\cos(\Omega_1 t)\sin\left(\frac{2\pi x}{a}\right)\sin\left(\frac{\pi y}{b}\right) \tag{29}$$

$$N_{ti}=N_{ti1}(t)\cos(\Omega_2 t)\sin\left(\frac{\pi x}{2a}\right)\cos\left(\frac{\pi y}{b}\right)+N_{ti2}(t)\cos(\Omega_2 t)\sin\left(\frac{3\pi x}{2a}\right)\cos\left(\frac{2\pi y}{b}\right),i=1,2 \tag{30}$$

$$N_{pi}=N_{pi1}(t)\cos(\Omega_3 t)\sin\left(\frac{\pi x}{2a}\right)\cos\left(\frac{\pi y}{b}\right)+N_{pi2}(t)\cos(\Omega_3 t)\sin\left(\frac{3\pi x}{2a}\right)\cos\left(\frac{2\pi y}{b}\right),i=1,2 \tag{31}$$

根据图 2 的模型,MFC-GP 板在振动过程中,起主导作用的为横向位移,所以,这里主要研究横向位移. 利用 Galerkin 法对得到无量纲后的两个自由度常微分方程:

$$\ddot{w}_1+\mu_1\dot{w}_1+k_{11}w_1^3+k_{12}w_2^3+k_{13}w_1^2w_2+k_{14}w_1w_2^2+\omega_1^2w_1+(t_{11}\cos(\Omega_2 t)+p_{11}\cos(\Omega_3 t))w_1+(t_{12}\cos(\Omega_2 t)+p_{12}\cos(\Omega_3 t))w_2=k_{15}F_1\cos(\Omega_1 t) \tag{32}$$

$$\ddot{w}_2+\mu_2\dot{w}_2+k_{21}w_1^3+k_{22}w_2^3+k_{23}w_1^2w_2+k_{24}w_1w_2^2+\omega_2^2w_2+(t_{21}\cos(\Omega_2 t)+p_{21}\cos(\Omega_3 t))w_1+(t_{22}\cos(\Omega_2 t)+p_{22}\cos(\Omega_3 t))w_2=k_{25}F_2\cos(\Omega_1 t) \tag{33}$$

其中,$\mu_i(i=1,2)$为阻尼系数,$k_{ij}(i=1,2;\ j=1,2,3,4)$为非线性项系数,$t_{ij}$、$p_{ij}(i=1,2;\ j=1,2)$分别为温度系数,压电系数.

3　摄动分析

利用多尺度方法对方程(32)~(33)进行摄动分析,引入小参数 ε,设方程的解有如下形式:

$$w_1=w_{10}(T_0,T_1)+\varepsilon w_{11}(T_0,T_1)+\cdots \tag{34}$$

$$w_2=w_{20}(T_0,T_1)+\varepsilon w_{21}(T_0,T_1)+\cdots \tag{35}$$

考虑基本参数共振和 1:1内共振,关系如下所示:

$$\omega_1=\Omega_1-\varepsilon\sigma_1,\omega_2=\Omega_1-\varepsilon\sigma_2,\Omega_1=1,\Omega_2=\Omega_3=2 \tag{36}$$

其中,ω_1,ω_2 是系统前两阶线性固有频率;σ_1,σ_2 是两个频率调谐参数.

将(34)~(36)带入到(32)~(33)中,使 ε 同阶系数项系数相等,可得到 ε^0 阶和 ε^1 阶.

ε^0 阶:

$$D_0^2w_{10}+w_1^2w_{10}=0 \tag{37}$$

$$D_0^2w_{20}+w_1^2w_{20}=0 \tag{38}$$

ε^1 阶:

$$D_0^2w_{11}+w_1^2w_{11}=-2D_0D_1w_{10}-\mu_1D_0w_{10}-k_{11}w_{10}^3-k_{12}w_{20}^3-k_{13}w_{10}^2w_{20}-k_{14}w_{10}w_{20}^2+2\Omega_1\sigma_1w_{10}-(t_{11}\cos(\Omega_2 t)+p_{11}\cos(\Omega_3 t))w_{10}-$$

$$(t_{12}\cos(\Omega_2 t)+p_{12}\cos(\Omega_3 t))w_{20}+k_{15}F\cos(\Omega_1 t) \tag{39}$$

$$D_0^2 w_{21}+w_2^2 w_{21}=-2D_0D_1w_{20}-\mu_2 D_0 w_{20}-k_{21}w_{10}^3-k_{22}w_{20}^3-k_{23}w_{10}^2w_{20}-k_{24}w_{10}w_{20}^2+2\sigma_2\Omega_1 w_{20}-(t_{21}\cos(\Omega_2 t)+p_{21}\cos(\Omega_3 t))w_{10}-(t_{22}\cos(\Omega_2 t)+p_{22}\cos(\Omega_3 t))w_{20}+k_{25}F\cos(\Omega_1 t) \tag{40}$$

设方程(39)~(40)解的形式如下：

$$w_{10}=A_1(T_1)e^{i\Omega_1 T_0}+cc \tag{41}$$

$$w_{20}=A_2(T_1)e^{i\Omega_1 T_0}+cc \tag{42}$$

其中，$A_1=\frac{1}{2}a_1e^{i\beta_1}$，$A_2=\frac{1}{2}a_2e^{i\beta_2}$.

将(41)~(42)带入到(39)~(40)，消除永年项，并进行实虚部分离，得到极坐标形式下的平均方程：

$$\dot{a}_1=-\frac{1}{2}\mu_1a_1-\frac{3}{8}k_{12}a_2^3\sin(\beta_2-\beta_1)+\frac{1}{8}k_{13}a_1^2a_2\sin(\beta_2-\beta_1)-\frac{1}{4}k_{13}a_1^2a_2\sin(\beta_2-\beta_1)-\frac{1}{8}k_{14}a_2^2a_1\sin(2(\beta_2-\beta_1))+\frac{1}{4}(t_{11}+p_{11})a_1\sin(2\beta_1)+\frac{1}{4}(t_{12}+p_{12})a_2\sin(\beta_1+\beta_2)-\frac{k_{15}F}{2}\sin(\beta_1) \tag{43}$$

$$a_1\dot{\beta}_1=\frac{3}{8}k_{11}a_1^3+\frac{3}{8}k_{12}a_2^3\cos(\beta_2-\beta_1)-\frac{1}{8}k_{13}a_1^2a_2\cos(\beta_2-\beta_1)+\frac{1}{4}k_{13}a_1^2a_2\cos(\beta_2-\beta_1)+\frac{1}{8}k_{14}a_2^2a_1\cos(2(\beta_2-\beta_1))+\frac{1}{4}k_{14}a_2^2a_1-\sigma_1a_1+\frac{1}{4}(t_{11}+p_{11})a_1\cos(2\beta_1)+\frac{1}{4}(t_{11}+p_{11})a_2\cos(\beta_1+\beta_2)-\frac{k_{15}F}{2}\cos(\beta_1) \tag{44}$$

$$\dot{a}_2=-\frac{1}{2}\mu_2a_2-\frac{3}{8}k_{21}a_2^3\sin(\beta_1-\beta_2)-\frac{1}{8}k_{23}a_1^2a_2\sin(2(\beta_1-\beta_2))+\frac{1}{8}k_{24}a_2^2a_1\sin(\beta_1-\beta_2)-\frac{1}{4}k_{24}a_2^2a_1\sin(\beta_1-\beta_2)+\frac{1}{4}(t_{21}+p_{21})a_1\sin(\beta_1+\beta_2)+\frac{1}{4}(t_{22}+p_{22})a_2\sin(2\beta_2)-\frac{k_{25}F}{2}\sin(\beta_2) \tag{45}$$

$$a_2\dot{\beta}_2=\frac{3}{8}k_{21}a_1^3\cos(\beta_1-\beta_2)+\frac{3}{8}k_{22}a_2^3+\frac{1}{8}k_{23}a_1^2a_2\cos(2(\beta_1-\beta_2))+\frac{1}{4}k_{23}a_1^2a_2-\frac{1}{8}k_{24}a_2^2a_1\cos(\beta_1-\beta_2)+\frac{1}{4}k_{24}a_2^2a_1\cos(\beta_1-\beta_2)-\sigma_2a_2+\frac{1}{4}(t_{21}+p_{21})a_1\cos(\beta_1+\beta_2)+\frac{1}{4}(t_{22}+p_{22})a_2\cos(2\beta_2)-\frac{k_{25}F}{2}\cos(\beta_2) \tag{46}$$

考虑结构具有定常双振子解，得到结构的频响函数

$$\left(-\frac{1}{2}\mu_1a_1+\frac{1}{4}(t_{11}+p_{11})a_1\sin(2\beta_1)+\frac{1}{4}(t_{12}+p_{12})a_2\sin(\beta_1+\beta_2)-\frac{k_{15}F}{2}\sin(\beta_1)\right)^2+\left(\frac{3}{8}k_{11}a_1^3+\frac{1}{8}k_{14}a_2^2a_1-\sigma_1a_1+\frac{1}{4}(t_{11}+p_{11})a_1\cos(2\beta_1)+\frac{1}{4}(t_{11}+p_{11})a_2\cos(\beta_1+\beta_2)-\frac{k_{15}F}{2}\cos(\beta_1)\right)^2=\left(-\frac{3}{8}k_{12}a_2^3-\frac{1}{8}k_{13}a_1^2a_2-\frac{1}{4}k_{14}a_2^2a_1\cos(\beta_2-\beta_1)\right)^2 \tag{47}$$

$$\left(-\frac{1}{2}\mu_2a_2+\frac{1}{4}(t_{21}+p_{21})a_1\sin(\beta_1+\beta_2)+\frac{1}{4}(t_{22}+p_{22})a_2\sin(2\beta_2)-\frac{k_{25}F}{2}\sin(\beta_2)\right)^2+\left(\frac{3}{8}k_{22}a_2^3+\frac{1}{8}k_{23}a_1^2a_2-\sigma_2a_2+\frac{1}{4}(t_{21}+p_{21})a_1\cos(\beta_1+\beta_2)+\frac{1}{4}(t_{22}+p_{22})a_2\cos(2\beta_2)-\frac{k_{25}F}{2}\cos(\beta_2)\right)^2=\left(-\frac{3}{8}k_{21}a_1^3-\frac{1}{4}k_{23}a_1^2a_2\cos(\beta_1-\beta_2)-\frac{1}{8}k_{24}a_2^2a_1\right)^2 \tag{48}$$

4 数值模拟

本节根据上述得到的振动控制方程及频响函数分析结构的非线性振动特性. MFC-GP 复合材料板的物理参数如表 1 所示，几何参数为 $a=1.5$m，

$b=1\mathrm{m}$,$h=0.002\mathrm{m}$,电压参数 $U=1\mathrm{kV}$,温度参数 $\Delta T=500℃$.

考虑方程(47)中 $a_2=1$ 及方程(48)中 $a_1=1$,得到结构随石墨烯体积分数变化的频响曲线如图 4、5 所示.从图 4~5 中可以看出,一、二阶模态均呈现硬弹簧特性,且随着石墨烯体积分数的增加,硬弹簧特性越来越明显.

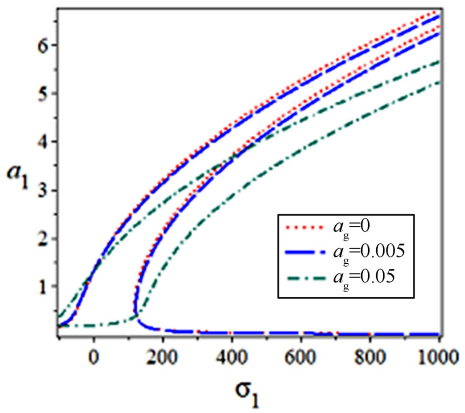

图 4　一阶模态的频响曲线随石墨烯体积分数的变化

Fig.4　Frequency-response curves of the first-order mode under different GP volume fractions

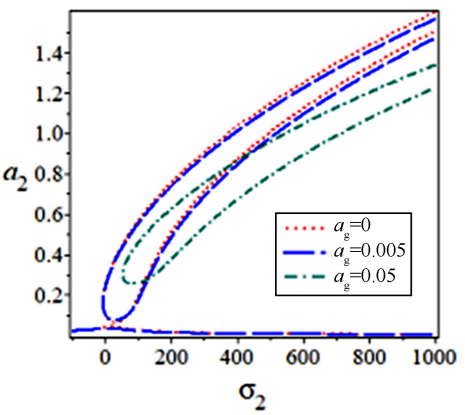

图 5　二阶模态的频响曲线随石墨烯体积分数的变化

Fig.5　Frequency-response curves of the second-order mode under different GP volume fractions

当石墨烯体积分数为 0.005 时,研究电压、温度、初相位对频响曲线的影响,结果如图 6~11 所示.图 6、7 表明随着电压的增加,频响曲线变化较小. 图 8、9 表明随着温差的增加,共振区域变小,并当温度继续增大时,一阶模态的跳跃现象消失. 同时,初相位对频响曲线的影响也比较大,当初相位由负变为正的过程中,共振区域逐渐增加,如图 10、11 所示.

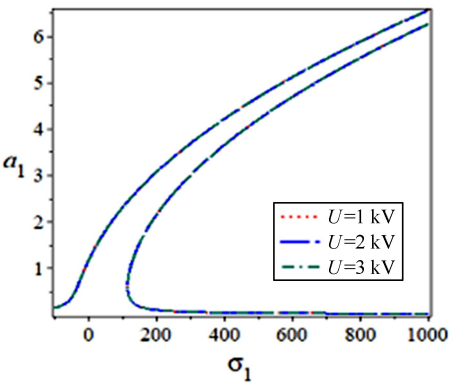

图 6　一阶模态的频响曲线随电压的变化

Fig.6　Frequency-response curves of the first-order mode under different voltages

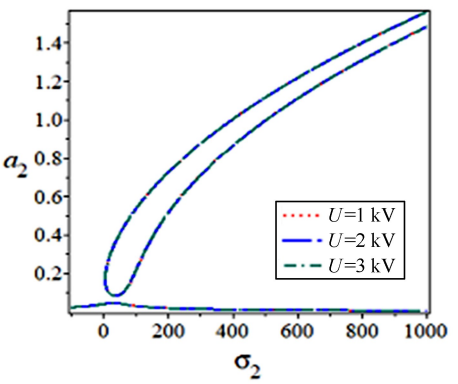

图 7　二阶模态的频响曲线随电压的变化

Fig.7　Frequency-response curves of the second-order mode under different voltages

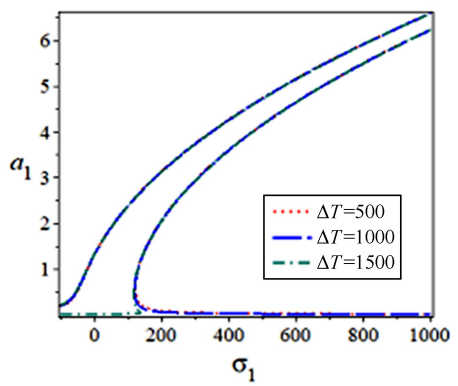

图 8　一阶模态的频响曲线随温度的变化

Fig.8　Frequency-response curves of the first-order mode under different temperature

下面采用 Runge-Kutta 法对 MFC-GP 板进行数值模拟,结构的物理参数如上表 1 所示.研究石墨烯体积分数 0.005,$U=1\mathrm{kV}$,$\Delta T=500℃$时,外激励对结构非线性振动响应的影响.通过图 12 发现,当外激励从 0 到 160N 的过程中,结构经历了混沌运

动—周期运动—混沌运动—周期运动—混沌运动交替的过程. 同时给出了系统在不同外激励作用下发生周期和混沌运动的具体形式,图 13 为外激励 $F=82$N 时,结构发生的多倍周期运动,图 14 为外激励 $F=110$N 时结构发生的混沌运动,其中图(a)和(b)是结构在(x_1,x_2)和(x_3,x_4)的相图,图(c)和(d)是$(t,\ x_1)$和(t,x_3)上的波形图,图(e)是三维相图.

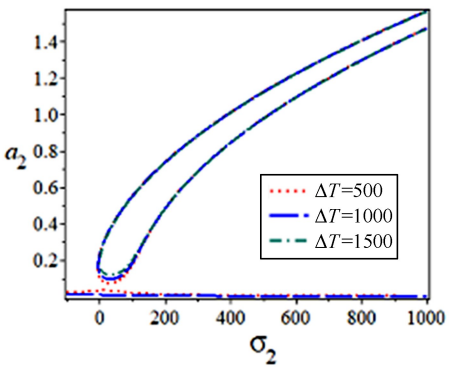

图 9 二阶模态的频响曲线随温度的变化

Fig.9 Frequency-response curves of the second-order mode under different temperature

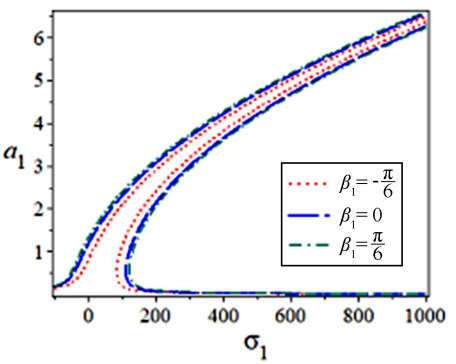

图 10 一阶模态的频响曲线随初相位的变化

Fig.10 Frequency-response curves of the first-order mode under different initial phase

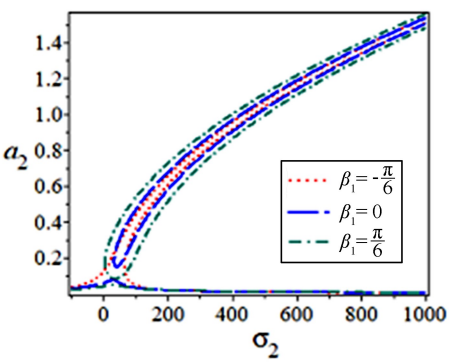

图 11 二阶模态的频响曲线随初相位的变化

Fig.11 Frequency-response curves of the second-order mode under different initial phase

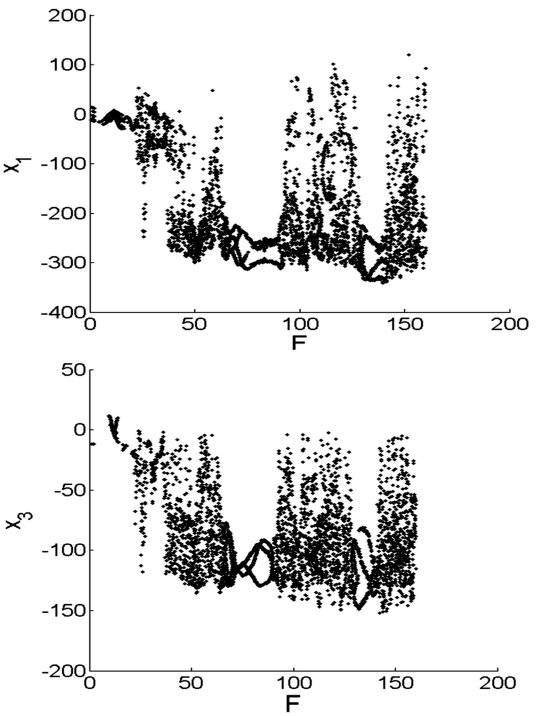

图 12 结构的分叉图

Fig.12 Bifurcation diagram of the structure

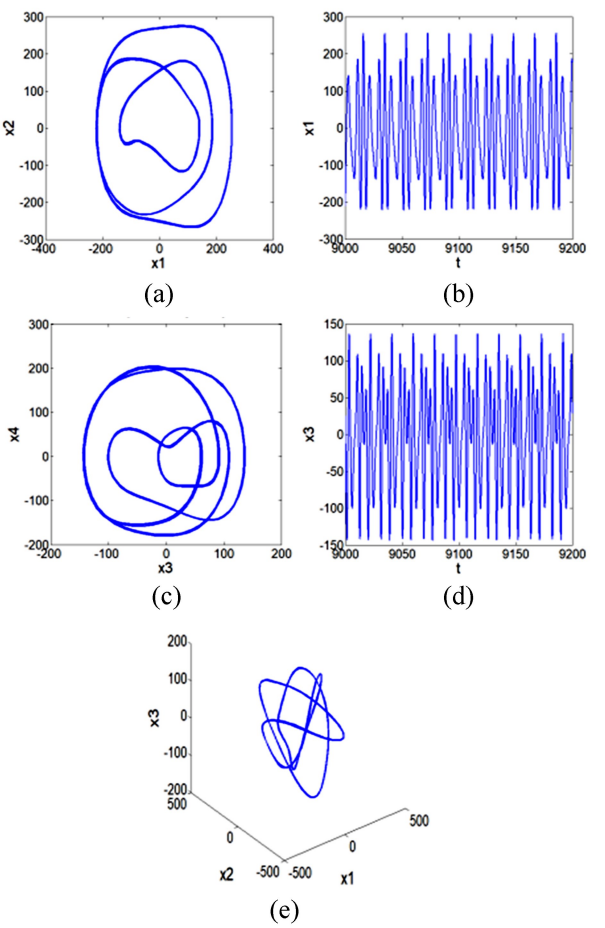

图 13 MFC-GP 板的多倍周期运动

Fig.13 Periodic-n motions of the MFC-GP plate

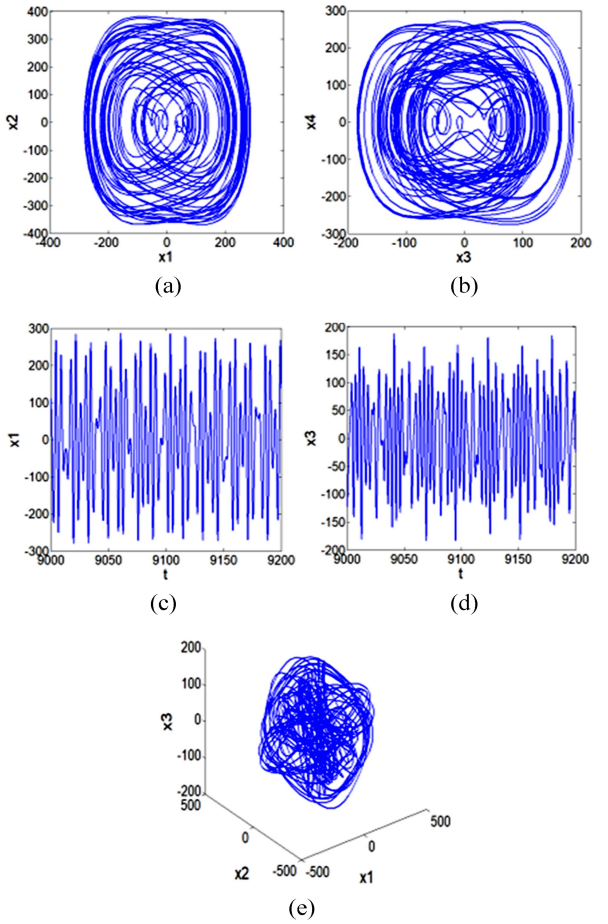

图 14　MFC-GP 板的混沌运动

Fig.14　Chaotic motion of the MFC-GP plate

同时,一些其他的因素也会对结构的振动产生较大的影响,比如: 阻尼、初值等.参数如表 1 不变,当阻尼系数由 0.005 变成 0.001 时,结构的振动响应如图 15 所示,随着阻尼变小,不稳定区域增加.当初值由[1.44,1.55,-2.35,1.779]变成[0.44,0.55,1.35,0.779]时,结构的响应如图 16 所示,结构的动态稳定区域增加.

5　结论

本文研究了带有石墨烯涂层的 1-3 型压电纤维复合材料(MFC-GP)简支板结构的非线性动力学特性. 基于 Reddy 一阶剪切变形理论, Von Kármán 位移应变关系,Hamilton 原理得到 MFC-GP 板在广义位移下的非线性动力学方程. 利用 Galerkin 法对无量纲化后的方程进行离散,得到一个自由度的常微分方程. 利用特征值法,得到不同 m、n 情况下的固有频率. 采用多尺度法进行摄动分析,研究结构在基本参数共振和 1∶1内共振的情况下的动

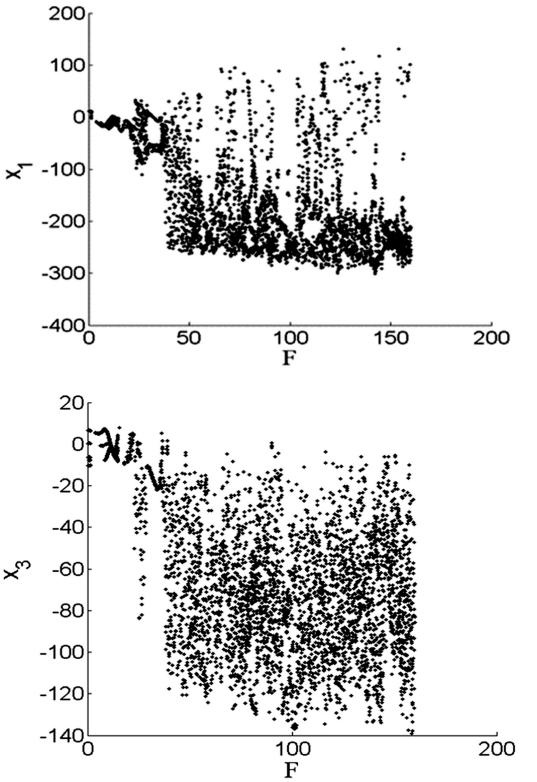

图 15　改变阻尼的结构分叉图

Fig.15　Changing damping coefficients of the Structural bifurcation diagram

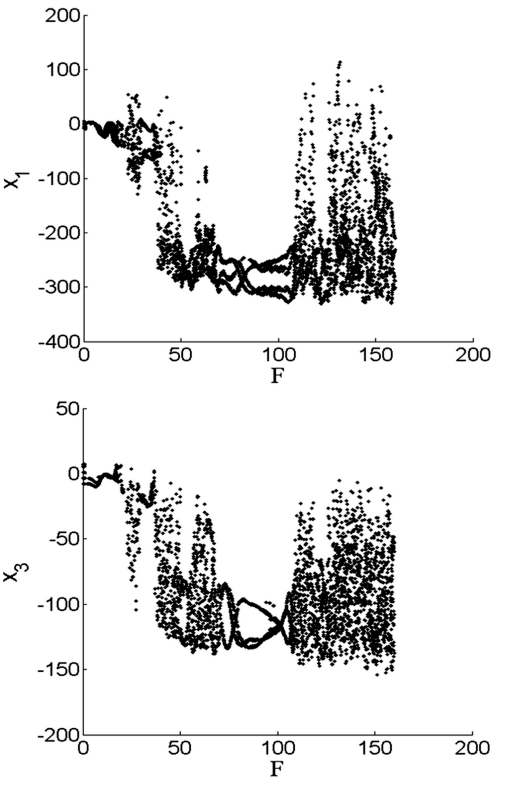

图 16　改变初值的结构分叉图

Fig.16　Changing the initial conditions of the Structural bifurcation diagram

态稳定性. 数值结果表明,结构呈现硬弹簧特性,随着石墨烯体积分数的增加. 硬弹簧特性明显. 同时还研究了电压、温度、初相位对频响曲线的影响. 结果表明,电压的改变对结构的振动响应影响较小,随着温度的增加,共振区域变小,且当温度增加到一定时,结构的跳跃现象消失. 初相位对结构也具有一定的影响,当初相位从负变为正的过程中,结构的共振区域增大.

同时,采用 Runge-Kutta 法对结构进行了数值模拟,得到了结构的分叉图、相图、波形图以及三维相图. 结果表明,随着外激励大小的改变,结构依次出现了混沌运动—周期运动—混沌运动交替的过程. 同时,阻尼和初值对结构的振动响应也比较大,改变阻尼的大小,可改变结构的稳定性,使不稳定区域增加,改变初值可改变结构的稳定区域.

参 考 文 献

1 曾尤,王涵,成会明. 石墨烯/聚合物复合材料的研究及其应用前景进展. 新型碳材料,2012,31(6):555~567 (Zeng Y, Wang H, Cheng H M. Research progress and potential applications for graphene/polymer composites. *New Carbon Materials*, 2012, 31(6): 555~567 (in Chinese))

2 Tang Y P, XuQ, Tang R Z, et al. Preparation and applications of two dimensional carbon materials. *Carbon*, 2016, 110:518

3 Adak N C, Chhetri S, Kim N H, et al. Static and dynamic mechanical properties of graphene oxide-incorporated woven carbon fiber/epoxy composite. *Journal of Materials Engineering and Performance*, 2018, 27(3): 1138~1147

4 Shen H S, Lin F, Xiang Y. Nonlinear vibration of functionally graded graphene-reinforced composite laminated beams resting on elastic foundations in thermal environments. *Nonlinear Dynamics*, 2017, 90(2): 899~914

5 Shahrjerdi A, Yavari S. Free vibration analysis of functionally graded graphene-reinforced nanocomposite beams with temperature-dependent properties. *Journal of the Brazilian Society of Mechanical Sciences and Engineering*, 2018, 40(1)

6 Li H B, Wang X. Nonlinear frequency shift behavior of graphene-elastic-piezoelectric laminated films as a nano-mass detector. *International Journal of Solids and Structures*, 2016, 84: 17~26

7 Xu K, Wang K, Zhao W, et al. The positive piezoconductive effect in graphene. *Nature Communications*, 2015, 6: 8119

8 Phiri J, Johansson L S, Gane P, et al. A comparative study of mechanical, thermal and electrical properties of graphene-, graphene oxide- and reduced graphene oxide-doped microfibrillated cellulose nanocomposites. *Composites Part B: Engineering*, 2018, 147: 104~113

9 Guo X Y, Jiang P, Zhang W, et al. Nonlinear dynamic analysis of composite piezoelectric plates with graphene skin. *Composite Structures*, 2018, 206: 839~852

10 李敏,陈伟民,贾丽杰. 压电纤维复合材料铺层用于翼面设计的驱动特性与刚度影响. 航空学报,2010,31(2):418~425 (Li M, Chen W M, Jia L J. Drive Characteristics and Stiffness Influence with Piezoelectric Fiber Composite Actuators on Airfoil Surface. *Acta Aeronautica Et Astronautica Sinica*, 2010, 31(2): 418~425 (in Chinese))

11 郭翔鹰,刘大猛,张伟. 压电纤维复合材料层合壳的非线性动力学研究. 动力学与控制学报,2017,15(5):430~439 (Guo X Y, Liu D M, Zhang W. Nonlinear dynamic analysis of piezoelectric macro-fiber composite laminated shells. *Journal of Dynamics and Control*, 2017, 15(5): 430~439 (in Chinese))

12 杨佳慧,张伟,袭安. 压电复合材料悬臂板 1:3内共振的非线性动力学分析. 动力学与控制学报,2018,16(5):440~448 (Yang J H, Zhang W, Xi A. Nonlinear dynamic analysis of a composite cantilever piezoelectric plate with one-to-three internal resonance. *Journal of Dynamics and Control*, 2018, 16(5): 440~448 (in Chinese))

13 Ray M C, Reddy J N. Active control of laminated cylindrical shells using piezoelectric fiber reinforced composites. *Composites Science & Technology*, 2005, 65(7): 1226~1236

14 Rafiee M, Liu X F, He X Q, et al. Geometrically nonlinear free vibration of shear deformable piezoelectric carbon nanotube/fiber/polymer multiscale laminated composite plates. *Journal of Sound & Vibration*, 2014, 333(14): 3236~3251

15 Vlassiouk I, Polizos G, Cooper R, et al. Strong and electrically conductive graphene-based composite fibers and laminates. *ACS Applied Materials and Interfaces*, 2015, 7(20): 10702~10709

16 赵明慧,张伟. 矩形复合材料悬臂板的非线性动力学分

析. 中国力学大会暨钱学森诞辰 100 周年纪念大会, 2011 (Zhao M, Zhang W. Nonlinear dynamics of composite laminated cantilever rectangular plate. Chinese mechanics congress and the 100th anniversary of Qian Xuesen's birth, 2011 (in Chinese))

NONLINEAR DYNAMICS OF A THREE-PHASE COMPOSITE MATERIALS PLATE WITH GRAPHENE *

Jiang Pan　Guo Xiangying†　Zhang Wei

(*College of Mechanical Engineering, Beijing University of Technology, Beijing* 100124, *China*)

Abstract In this paper, the nonlinear dynamic characteristics of simple supported plate structures of 1-3 type piezoelectric fiber composites (MFC-GP) coated with graphene were studied. First, the nonlinear partial differential equation of the MFC-GP composite material plate was deduced based on the Reddy first-order shear deformation theory, Von Kármán displacement strain relation and Hamilton principle. Then, it was discretized into two-degree-of-freedom ordinary differential equation by the Galerkin method. Furthermore, the frequency-response equation with internal resonance 1:1 was obtained by the multi-scale method, and the effects of volume fraction of graphene, voltage, temperature and initial phase on the frequency response curve were analyzed. Finally, the vibration response of MFC-GP composite plate was investigated by using bifurcation diagram, phase diagram and waveform through numerical simulations. The results were shown complex nonlinear vibrations of the plate with different parameters and external excitations, which would have certain guiding significance for future engineering application.

Key words MFC-GP composite plate, internal resonance, frequency response curve, nonlinear vibration

Received 4 November 2018, revised 12 December 2018.

* The project supported by the National Natural Science Foundation of China (11772010, 11572006, 11602234).

† Corresponding author E-mail: eagle2008guo@yeah.net

附录 A

$$M_i=\frac{a_g g_{3gi}\bar{s}_i+(1-a_g)\bar{g}_{3pmi}s_i}{(1-a_g)s_i+a_g\bar{s}_i}\quad(i=1,2)$$

$$N_i=a_g\beta_{33g}^T+(1-a_g)\bar{\beta}_{33pm}^T+\frac{a_g(g_{3gi})^2}{s_i}+\frac{(1-a_g)(\bar{g}_{3pmi})^2}{\bar{s}_i}-\left[\frac{a_g g_{3gi}}{s_i}+\frac{(1-a_g)\bar{g}_{3pmi}}{\bar{s}_i}\right]\left[\frac{a_g g_{3gi}\bar{s}_i+(1-a_g)\bar{g}_{3pmi}s_i}{a_g\bar{s}_i+(1-a_g)s_i}\right]\quad(i=1,2)$$

$$\beta_{33g}^T=\frac{1}{\varepsilon_{33}^T}$$

$$g_{3gi}=\frac{d_{3gi}}{\varepsilon_{33}^T}\quad(i=1,2)$$

$$\bar{g}_{3pmi}=\frac{a_p\left[d_{3pi}-\frac{(1-a_p)d_{33p}(s_{13}^{Ep}-s_{12}^{Em})}{s(a)}\right]}{\left[a_p\varepsilon_{33}^{Tp}-\frac{a_p(1-a_p)d_{33p}^2}{s(a)}+(1-a_p)\varepsilon_{11}^{Tm}\right]}\quad(i=1,2)$$

$$\bar{\beta}_{33pm}^T=\frac{1}{\left[a_p\varepsilon_{33}^{Tp}-\frac{a_p(1-a_p)d_{33p}^2}{s(a)}+(1-a_p)\varepsilon_{11}^{Tm}\right]}$$

$$s(a)=a_p s_{11}^{Em}+(1-a_p)s_{33}^{Ep}$$

$$\bar{s}_i=a_p(s_{11}^{Ep}+s_{12}^{Ep})+(1-a_p)(s_{11}^{Em}+s_{12}^{Em})-s_3-s_{4i}\quad(i=1,2)$$

附录 B

$$a_{11}=A_{11},a_{12}=A_{11},a_{13}=A_{12}+A_{66},a_{14}=A_{12}+A_{66},$$
$$a_{15}=A_{66},a_{16}=A_{66},a_{17}=I_0,a_{18}=-I_1$$
$$b_{11}=A_{22},b_{12}=A_{22},b_{13}=A_{12}+A_{66},b_{14}=A_{12}+A_{66}$$
$$b_{15}=A_{66},b_{16}=A_{66},b_{17}=I_0,b_{18}=-I_1$$
$$c_{11}=2A_{12}+4A_{66},c_{12}=A_{66},c_{13}=A_{12},c_{14}=A_{11},$$
$$c_{15}=A_{66}+\frac{1}{2}A_{12},c_{16}=A_{11},c_{17}=2A_{66},$$
$$c_{18}=A_{66}+\frac{1}{2}A_{12},c_{19}=\frac{3}{2}A_{11},c_{20}=A_{22}$$
$$c_{21}=A_{12}+A_{66},c_{22}=A_{12}+A_{66},c_{23}=\frac{3}{2}A_{22},c_{24}=A_{22},$$
$$c_{25}=A_{12},c_{26}=A_{66},c_{27}=2A_{66},c_{28}=N_{t1}+N_{e1},$$
$$c_{29}=N_{t2}+N_{e2},c_{30}=-D_{11},c_{31}=-2D_{12}-4D_{66}$$
$$c_{32}=-D_{22},c_{33}=r,c_{34}=I_0,c_{35}=I_1,c_{36}=I_1$$
$$c_{37}=-I_2,c_{38}=-I_2$$